Journal of Applied Sciences

ISSN 1812-5654

science alert

ANSInet
an open access publisher
http://ansinet.com

Journal of Applied Sciences 8 (23): 4238-4250, 2008
ISSN 1812-5654

The Role of Shear Zone on the Emplacement of Malayer Granitoid Rocks, NW Iran

V. Ahadnejad, M.V. Valizadeh and D. Esmaeily
Department of Geology, University College of Science, University of Tehran, Iran

Abstract: Malayer complex is emplaced within the early to middle Jurassic regional metamorphic rocks which consist of slate, phyllite and schist so called Hamadan phyllite in the Sanandaj-Sirjan Zone (SSZ). The Sanandj-Sirjan Zone is produced by oblique collisional event between Arabian plate and Central Iran microcontinent. The Malayer plutonic complex, in the Northern Sanandj-Sirjan Zone (Western Iran), is a composite, roped-shaped intrusive body, range from alkali granite, syenogranite, monzogranite, granodiorite, to tonalite in composition with high-K calc-alkaline affinity and some little massives of basic-to-intermediate, gabbro and diorite that have different geological history. They typically have angular to spherical-shaped magmatic and metamorphic enclaves. A persistent control on the emplacement of the various suites by a nearby oblique, strike-slip pressional is suggested by several features. Among them are: (a) shapes of individual intrusions and their location in transpressional sites (b) metric to decimetric-thick sheets emplaced along shear bands (c) fold axial surfaces (d) transitions between viscous- to solid-state fabrics in the pluton and (e) bearing the same orientation and kinematics as in their country rocks. Furthermore, intergrowth textures such as myrmekite and perthite, mylonitic granites, complex deformation and elongated shape imply injection of melt along the high-strain shear zone.

Key words: Oblique collision, subduction, mylonite, sanandaj-sirjan metamorphic belt, dextral transpression regime

INTRODUCTION

Extraction of granitic magma from lower crust and its emplacement at shallower levels, is the principal mechanism by which the continents have become differentiated. Thus, understanding how magma moves through the crust is an important step toward understanding crustal evolution. The processes controlling granitic magma transport and emplacement in the crust are all controversial. Gravity is the essential driving force for large-scale vertical transport of melts (ascent) in the continental crust (Petford *et al*., 2000). However, the traditional idea of buoyant granitic magma ascending through the continental crust as slow-rising, hot diapirs or by stoping (that is, large-scale veining) (Weinberg and Podladchikov, 1994) has been largely replaced by more viable models (Snelling, 2008). These models involve the very rapid ascent of granitic magmas in narrow conduits, either as self-propagating dykes (Clemens *et al*., 1997), along preexisting faults (Petford *et al*., 1993), or as an interconnected network of active shear zones and dilational structures (Collins and Sawyer, 1996; D'Lemos *et al*., 1993).

However, in many convergent orogenic belts spatial and temporal relationships between granite and regional tectonic structures suggest ascent and emplacement during contraction rather than during extension (Hutton, 1997; Brown and Solar, 1998). During orogenesis, melting occurs in a dynamic environment in which differential stresses acting upon anisotropic crust lead to heterogeneous deformation at all scales, which enables granite extraction, ascent and emplacement. In spite of the relationship between emplacement of granite and its deformation along shear zones or faults has generated a heated debate (Paterson and Schmidt, 1999), this geological feature is one of the most usual granite emplacement tectonic features. It has been argued that granites can migrate from their source to the mid-crust through relatively narrow shear zones. Vigneresse and Tikoff (1999) and Vigneresse and Clemens (2000) have argued that deformation is necessary for magma ascent. According to Vigneresse and Tikoff (1999), strain partitioning causes horizontal migration of melt into shear bands while the shear bands act as vertical conduits allowing melt migration to higher structural levels. Deformation-assisted pumping of melt is believed to be the mechanism by which this upward migration can take place.

Shear zones involve volumes of rock deformed by shearing stress under brittle-ductile or ductile conditions,

Corresponding Author: Vahid Ahadnejad, Department of Geology, University College of Science, University of Tehran, Iran
Tel: 0098 912 218 28 94 Fax: 0098 21 66 49 16 23

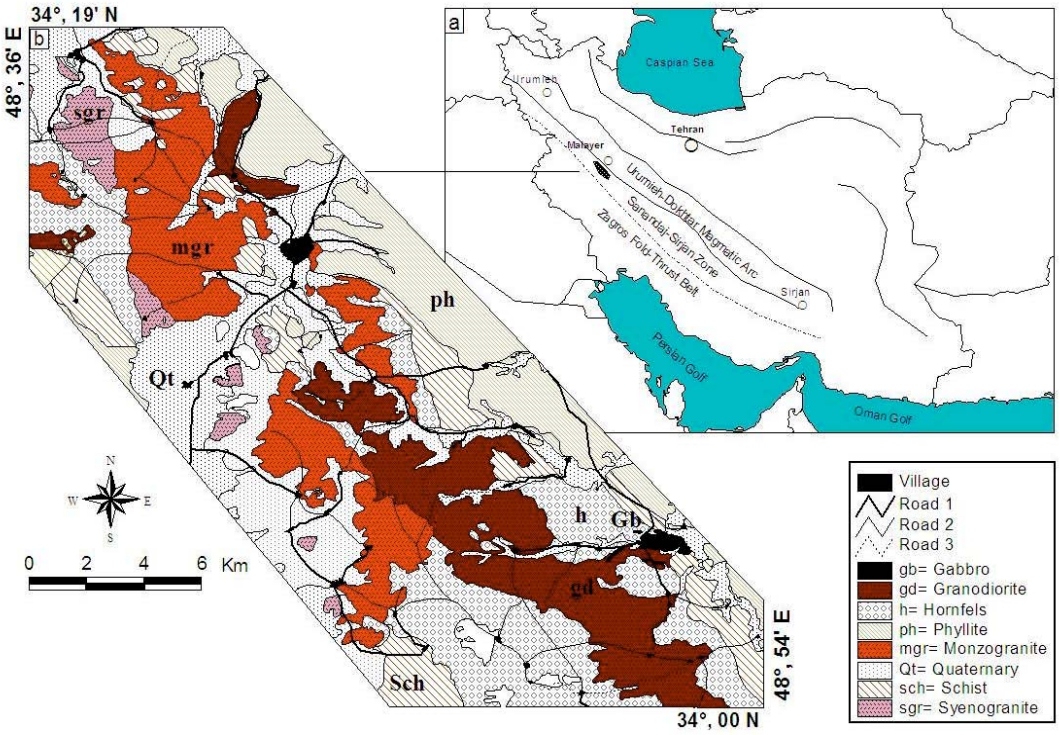

Fig. 1: (a) Major geological units of Western Iran and location of Malayer and (b) Malayer granitoids

typically in subduction zones at depths down to 10-20 km. Shear zones often occur at the edges of tectonic blocks, forming discontinuities that mark distinct terranes. They range from micrometer to kilometer scale, where they accommodate relative movement of tectonic units in orogenic belts. Shear zones are weaker than the surrounding rock and crustal deformation is believed to be largely determined by the rheology of shear zones (Sibson, 1977; White *et al*., 1980; Holdsworth *et al*., 1997).

In the interested area there are three major tectonic elements recognized in western and South-Western Iran that include the Urumieh-Dokhtar Magmatic Arc, the Zagros Fold-Thrust Belt and the Sanandaj-Sirjan Zone (Alavi, 1994). The Urumieh-Dokhtar Magmatic Arc is a long belt contains Tertiary-Quaternary intrusive and extrusive rocks (Berberian and Berberian, 1981). Continental collision occurred due to oblique convergent movement and non-orthogonal subduction of the Afro-Arabian continent toward Iranian microcontinent in upper cretaceous to miocene time (Mohajjel *et al*., 2003), with rates at 2.4 mm year^{-1} Hatzfeld *et al*. (2003) results important Zagros orogen. The presence of dextral shear sense indicators suggests that the Zagros Thrust System formed during triclinic dextral transpression in an inclined, obliquely convergent thrust wedge (Sarkarinejad and Azizi, 2007). This activity finalized at the Miocene by closure of the Thetyian oceanic crust and collision of North-Eastern margin of Arabia with Central Iran. The Sanandaj-Sirjan Zone (SSZ) has a length of 1500 km and a width up to 200 km. The main effects of mentioned collision in this zone is thrusting and highly deformation of rocks. These three zones are parallel to collision boundary which elongated across from North-West to Southeast Iran (Fig. 1).

The aim of this study is the assessment of transpression shear zone control on the emplacement of Malayer plutonic rocks in the Northern SSZ using microscopic and field data.

GEOLOGICAL SETTING

The SSZ is divided into two parts at the region of Golpayegan: Northern SSZ and Southern SSZ. Northern part includes Middle Jurassic to Miocene deformed intrusive rocks such as Alvand, Boroujerd and Malayer plutons and Southern part consists of rocks that deformed and metamorphosed in Middle to Late Triassic (Fig. 1). The geochemical, geochronological and petrogenesis studies of these plutons are poor and authors are studying the nature, origin, age and

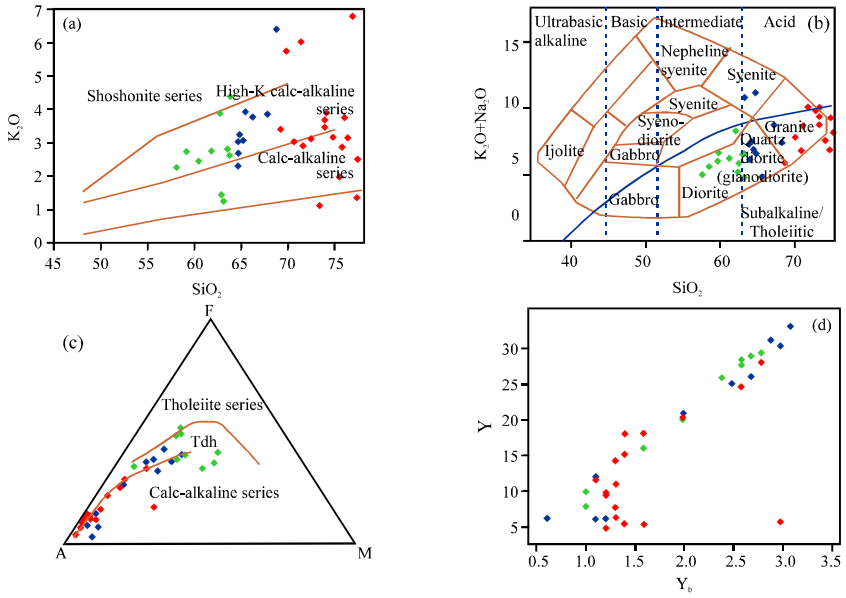

Fig. 2: (a) SiO_2 vs K_2O after Peccerillo and Taylor (1976), (b) The chemical classification and nomenclature of plutonic rocks using the total alkalis versus silica (TAS) diagram of Cox *et al.* (1979) adapted by Wilson (1989) for studied rocks. The curved solid line subdivides the alkali from subalkali rocks, (c) AFM plot from Irvine and Baragar (1971). The Tdh line corresponds to the differentiation trend of the standard trondhjemitic suite from Southwest Finland (Barker and Arth, 1976), Samples plot in the calc-alkaline field on the trondhjemitic trend and (d) Linear arrangement of Yb vs Y. Red square: Syenogranite; Blue square: Monzogranite; Green square: Granodiorite

emplacement mechanism of Malayer pluton. The general opinion is that they are arc-related calk-alkaline granitoids that form due to subduction of Neo-Thetys to Iranian Plate (Ahmadi-Khalaji *et al.*, 2006) but, contrary to general belief, new studies show more complication than this idea (Mazhari *et al.*, 2008). They demonstrate that the intrusive bodies age span from 40 Ma to 300 Ma.

The Malayer complex has NW-SE direction parallel to SSZ. The area covered by rocks is approximately 350 km^2; 35 km in length and 10 km in width. A diverse range of intrusive rocks found in this area and mapping and thin section investigations (Fig. 1, 2) prove that the Malayer is consist of three distinct intrusions: syenogranite, monzogranite and granodiorite. Some small patch of monzonite, diorite and gabbro exist between these unites. There are few felsic dykes with aplite and pegmatite composition. Nevertheless, no mafic dykes can bee seen. This region display a complex array of structural features including thrust faults, strik-slip faults and a variety of cleavages and foliations.

Regional metamorphic rocks are composed of various metasedimentary rocks with low to high grade metamorphism. Sedimentary rocks are metamorphosed during Late Kimmerian in the green schist facies and then at the Laramid orogenic phase these rocks underwent another deformation. Emplacement of Malayer granitic magma is coeval to the second deformation. Contact metamorphism has low effect and made narrow haloes. This may have several reasons: (a) rapid ascent and emplacement at the transpression tectonic regime (b) low temperature differences between country rocks and magma during emplacement and (c) low content of magmatic fluids which have important rule to heat transport.

GEOCHEMISTRY AND TECTONIC SETTING

Geochemical analyzes on some selected samples from the Chinamora Batholith have been performed to characterize possible sources of the granitoids and their genesis. Furthermore, the geochemical analyzes were used to classify the different samples and hence the different lithologies of the batholith according to different geochemical signatures. The element content of the samples was analyzed using an Inductively Coupled Plasma Mass Spectrometer (ICP-MS) and X-Ray Fluorescence Spectroscopy (XRF).

The Malayer granite has a variable composition, with SiO_2 contents of 58.28-77.35 wt.% (Table 1). These granitic intrusions are, in general, typical of high-K calc-alkaline magmas, although a few samples are potassic enough to

Table 1: Whole rock elemental analyses. Major oxides and LOI in wt.% and trace elements and REE in ppm

Sample	31	44	56	106	110	117	133	154	163	183	186	38
SiO_2	63.09	64.77	63.72	63.76	61.8	58.23	60.39	62.94	59.14	63.53	62.73	67.83
TiO_2	0.81	0.54	0.6	0.6	0.65	0.72	0.87	0.85	0.92	0.6	0.46	0.3
Al_2O_3	19.1	16.6	15.9	15.4	15.9	15.1	14.7	18.8	18	15.5	17.5	14.9
FeO	7.03	4.78	5.37	5.42	6.01	7.41	5.99	7.58	7.62	5.47	4.6	3.35
MnO	0.14	0.07	0.07	0.1	0.11	0.13	0.1	0.17	0.13	0.09	0.06	0.06
MgO	2.16	1.36	5.01	2.85	3.3	5.87	5.49	2.11	2.41	2.95	0.92	0.97
CaO	0.31	3.04	2.01	4.32	4.97	5.72	4.12	0.54	4.98	3.77	3.31	1.85
Na_2O	4.29	3.94	0.242	3.66	3.28	2.63	3.96	3.61	2.76	3.49	4.08	4.61
K_2O	1.27	3.21	4.37	2.64	2.73	2.23	2.41	1.42	2.7	2.8	3.88	3.83
P_2O_5	0.165	0.16	0.143	0.142	0.157	0.138	0.202	0.209	0.264	0.139	0.107	0.129
LOI	1.37	0.91	2.66	0.86	0.73	1.48	1.13	1.64	0.67	1.38	1.92	2.17
Ba	359	935	70	537	532	527	556	459	757	541	1410	639
Rb	234	180	9	161	166	144	221	157	123	153	134	229
Sr	87	285	247	294	314	278	201	106	289	301	380	182
Th	13	22	16	14	14	11	21	12	4	17	17	30
Zr	320	341	150	129	120	151	168	134	174	280	297	110
Ni	55	15	24	30	37	100	145	59	20	35	7	11
Sc	15	11	17	18	21	27	21	15	22	17	11	8
V	166	61	100	106	126	177	127	163	130	115	38	40
Pb	20	12	3	11	11	22	18	31	5	12	10	5
Cr	134	62	83	71	88	217	285	108	45	126	47	42
Co	16	10	10	14	17	25	24	18	16	15	7	6
Cu	10	8	1	13	20	28	44	16	7	13	7	5
Mo	0	1	1	0	1	0	0	1	0	2	1	1
Zn	125	64	45	58	57	87	69	122	95	58	43	35
Sn	4	1	2	1	1	2	3	3	2	1	1	1
Hf	6	7	7	5	8	7	7	6	5	9	6	5
W	7	3	2	0	0	1	2	1	0	1	0	3
La	34	49	37	35	31	32	53	37	17	33	71	54
Ce	76	99	80	71	65	65	105	74	34	65	129	98
Nd	22	29	26	24	23	19	18	28	23	24	26	27
Sm	4	7	5	4	3	3	3	3	4	4	6	7
Eu	1	2	1	1	1	1	2	1	1	1	1	2
Gd	5	5	5	5	5	5	5	5	6	4	6	4
Tb	1	1	1	1	1	1	1	1	1	1	1	1
Dy	3	4	5	6	6	6	6	4	3	6	4	6
Ho	1	1	1	1	1	1	1	1	1	1	1	1
Er	2	3	3	3	3	3	3	2	3	3	3	2
Tm	0	0	0	0	0	0	0	1	1	1	0	0
Yb	1	2	3	3	3	3	3	1	2	2	2	3
Lu	0	0	0	0	0	0	0	1	1	1	0	0
Y	8	20	28	28	29	27	34	10	16	26	20	26
Nb	12	14	11	10	11	10	13	13	13	10	11	14
Ta	1	1	1	1	1	1	1	1	1	1	1	1
Cs	18	8	0	4	7	8	16	15	8	6	8	3
Sample	54	68	80	126	127	134	157	161	164	187	188	189
SiO_2	66.28	65.42	69.24	64.62	63.86	74.77	65.22	65.29	64.68	68.79	70.71	75.42
TiO_2	0.59	0.5	0.37	0.57	1.16	0.02	0.54	0.17	0.69	0.51	0.34	0.1
Al_2O_3	15.3	15.8	15.4	15.5	19.9	15.1	16.6	19.7	16.9	17.8	14.5	13
FeO	4.64	3.95	3.54	4.67	0.38	0.98	4.88	0.9	5.62	0.62	3.3	1.28
MnO	0.08	0.07	0.06	0.09	0	0.07	0.08	0.01	0.11	0.02	0.05	0.02
MgO	2.44	2	1.2	2.4	0.92	0.11	1.59	1.01	1.75	0.34	0.76	0.38
CaO	3.82	2.37	2.32	3.75	1.69	0.5	3.37	0.82	2.44	3.46	1.36	1.88
Na_2O	0.903	2.44	2.36	2.81	0.407	4.2	3.59	0.134	3.64	0.663	4.53	4.67
K_2O	3.77	3.91	3.4	3.03	10	3.16	3.04	10.6	2.3	6.41	3.02	1.98
P_2O_5	0.131	0.203	0.164	0.13	0.514	0.35	0.162	0.271	0.161	0.136	0.079	0.026
LOI	1.97	3.23	1.66	2.24	1.09	0.48	0.74	0.82	1.63	0.77	1.09	1.02
Ba	406	401	433	456	49	60	594	13	486	70	1070	1620
Rb	40	123	119	131	11	147	139	10	184	28	132	103
Sr	568	215	317	283	86	30	274	36	160	559	314	292
Th	20	15	10	23	28	3	18	8	20	26	30	44
Zr	184	111	91	127	141	90	283	141	271	284	240	192
Ni	25	7	13	25	4	2	17	5	35	4	6	5
Sc	15	8	8	15	3	2	11	2	14	8	10	2
V	100	87	53	105	41	0	78	8	117	25	30	10
Pb	23	13	19	8	8	25	16	1	24	13	15	28
Cr	68	23	57	66	22	30	59	6	71	33	58	73
Co	10	9	8	12	1	1	10	2	14	1	5	3

Table 1: Continued

Sample	54	68	80	126	127	134	157	161	164	187	188	189
Cu	15	256	5	5	4	7	6	3	19	5	3	3
Mo	0	1	1	0	0	1	1	0	1	1	1	2
Zn	48	57	32	52	3	23	48	23	65	27	44	46
Sn	1	1	5	2	1	7	1	0	1	11	1	1
Hf	5	6	4	7	8	4	4	6	5	7	3	4
W	1	17	4	1	19	6	2	0	0	1	0	1
La	38	37	28	67	19	0	44	0	44	38	108	78
Ce	85	67	54	126	39	36	85	30	85	69	181	161
Nd	35	31	26	28	26	23	29	29	24	26	25	21
Sm	8	6	8	8	7	4	7	7	6	6	5	6
Eu	1	1	1	1	1	2	2	0	1	1	2	2
Gd	5	5	5	5	5	5	5	4	5	5	5	4
Tb	1	1	1	1	1	1	1	1	1	1	1	1
Dy	7	3	5	5	3	3	6	4	4	7	5	3
Ho	1	1	1	1	1	1	1	1	0	1	1	1
Er	3	1	4	2	2	7	2	3	2	2	3	3
Tm	0	0	1	0	1	0	0	0	1	0	0	0
Yb	3	1	2	3	1	1	3	1	1	3	3	2
Lu	0	0	1	0	0	0	0	0	1	0	0	0
Y	32	14	20	30	6	6	25	6	12	31	24	6
Nb	12	15	9	11	7	11	11	3	13	15	8	5
Ta	1	1	1	1	1	1	1	1	1	1	1	1
Cs	0	5	5	3	1	4	7	0	10	4	4	1

Sample	191	40	90	91	112	125	149	152	174	175	61	73	93	116	156	150
SiO_2	64.71	73.87	73.35	74.12	76.04	71.61	76.36	77.32	72.42	77.35	73.88	71.43	75.66	76.9	66.41	60.04
TiO_2	0.12	0.13	0.04	0.07	0.02	0.2	0.17	0.05	0.09	0.07	0.05	0.29	0.07	0.06	0.09	1.3
Al_2O_3	21.9	14.5	14.9	14.6	13.7	14.6	13.2	14.9	14.4	12.4	14.1	15.1	13.1	13.4	17.9	17.2
FeO	1.16	1.11	0.89	0.35	0.85	2.35	1.7	0.7	0.94	1.1	0.48	1.72	0.73	0.89	1.45	8.24
MnO	0.05	0.02	0.02	0	0.07	0.06	0.03	0.02	0.02	0.02	0	0.01	0.01	0.01	0.03	0.12
MgO	0.34	0.29	0.16	0.16	0.15	0.46	0.45	0.15	0.25	0.16	0.17	2.42	0.22	0.46	0.43	2.26
CaO	1.6	0.71	0.16	0.62	0.75	1.69	2.05	0.33	1.15	1.47	0.73	0.68	0.73	0.52	0.89	3.08
Na_2O	4.33	4.96	8.29	5.1	4.09	5.39	1.49	3.32	6.53	4.58	6	0.496	6.08	0.192	8.71	3.45
K_2O	2.67	3.48	1.12	3.88	3.75	2.9	3.14	1.37	3.14	2.47	3.66	6.04	2.85	6.8	2.44	2.47
P_2O_5	0.279	0.285	0.144	0.318	0.106	0.086	0.088	0.07	0.274	0.016	0.455	0.092	0.094	0.018	0.735	0.122
LOI	2.38	0.74	0.68	0.65	0.5	0.39	1.03	1.74	0.54	0.37	0.29	1.58	0.45	0.49	0.82	1.28
Ba	619	164	124	58	21	618	308	80	335	399	83	79	569	36	392	338
Rb	106	246	407	222	193	222	65	88	153	138	268	12	166	8	206	199
Sr	223	63	60	28	19	168	322	44	129	155	66	85	227	125	104	216
Th	4	6	2	3	4	29	46	4	3	17	2	20	33	24	5	67
Zr	181	145	125	100	187	164	121	102	111	214	128	124	108	81	78	112
Ni	5	4	3	0	0	5	12	2	17	5	3	7	3	2	3	31
Sc	3	2	4	2	0	6	5	2	2	3	2	9	1	3	4	25
V	14	6	2	2	0	20	18	4	8	7	4	34	7	3	8	79
Pb	81	44	47	23	37	22	34	28	23	20	24	3	14	2	86	20
Cr	42	13	30	8	13	37	30	23	46	48	31	20	25	16	18	58
Co	2	2	1	0	1	3	4	2	1	2	3	2	1	1	1	21
Cu	2	2	4	0	1	3	10	20	8	8	2	2	2	4	37	3
Mo	0	0	1	0	0	1	1	1	2	2	1	0	1	0	1	0
Zn	17	23	8	7	20	29	31	3	17	17	9	9	8	2	9	115
Sn	4	2	7	2	8	2	2	4	1	1	0	2	0	1	1	1
Hf	6	4	3	4	6	2	3	5	4	3	5	3	5	3	4	7
W	3	1	9	2	1	2	1	10	0	1	4	1	2	0	0	0
La	11	11	0	0	0	73	60	0	0	18	0	47	25	40	0	121
Ce	32	34	35	245	39	131	110	37	32	32	39	91	43	76	38	221
Nd	26	25	25	26	21	25	25	29	21	26	24	25	28	32	18	27
Sm	7	6	7	9	7	6	6	8	6	7	4	6	9	10	4	6
Eu	1	1	2	1	2	2	1	1	1	1	1	1	1	1	0	2
Gd	5	4	5	4	5	4	4	4	5	5	4	4	5	4	4	5
Tb	1	1	1	1	1	1	1	1	1	1	1	1	1	1	1	0
Dy	3	4	3	3	4	6	3	3	4	3	4	4	3	4	4	7
Ho	1	0	1	1	0	1	1	1	0	0	0	1	0	1	1	1
Er	2	2	5	6	2	3	3	4	4	2	2	2	3	2	2	5
Tm	0	0	0	1	1	1	1	1	0	0	0	1	0	1	0	0
Yb	1	1	1	1	1	3	1	3	1	1	1	2	1	1	1	3
Lu	0	0	0	1	1	1	1	1	0	0	0	0	0	1	0	0
Y	6	12	5	6	8	28	15	6	10	14	11	18	9	18	10	31
Nb	4	11	5	5	3	9	4	3	7	5	4	8	4	7	0	9
Ta	1	1	1	1	1	1	1	0	1	1	1	0	1	1	0	1
Cs	1	3	15	6	8	9	2	1	3	4	3	0	2	0	2	12

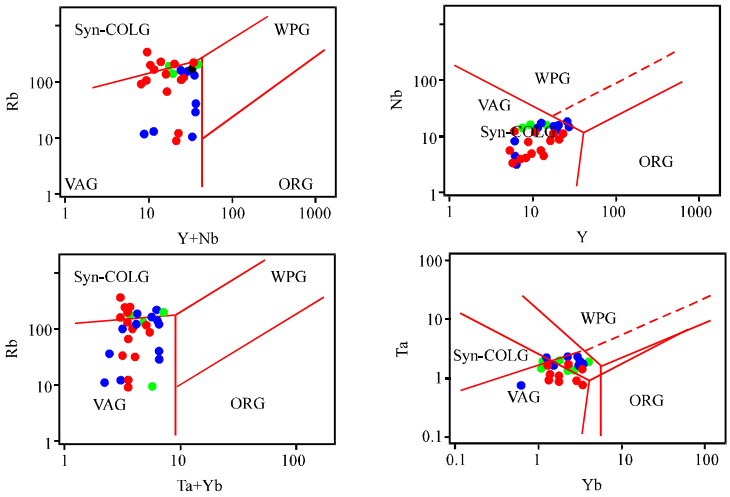

Fig. 3: Discrimination diagrams for the Malayer granite rocks. Syn-COLG: Syn-Collision Granite, VAG: Volcanic Arc Granite, WPG: Within-plate Granite, ORG: Ocean Ridge Granite. Field boundaries after Pearce *et al.* (1984)

plot in the extension of the low-K shoshonite field (Fig. 2a). The analyzed samples may be characterized according to their (Na_2O+K_2O) and their SiO_2 content (TAS-diagram of Cox *et al.* (1979). They are subalkaline (Fig. 2b) and most of the samples plot in the granite and granodiorit fields, where some of the samples may be characterized as alkali granites and some as granites. Only a few samples plot in the diorite and syenite fields.

On the trivariate plot of FeO(tot)-(Na_2O+K_2O)-MgO (AFM) (Irvine and Baragar, 1971) the samples plot close to the calc-alkaline trend and follow the trondhjemitic trend of Barker and Arth (1976) (Fig. 2c). Linear arrangement of tow incompatible elements indicated that the rock suit is co-magmatic (Fig. 2d). On the Rb-(Nb+Y) and Nb-Y discrimination diagrams of Pearce *et al.* (1984) the granitoid samples plot in the volcanic-arc and syn-colision granite fields (Fig. 3).

PETROGRAPHY

Microscopic analyzes have been performed on two sets of thin sections, one was cut according to the sample coordinates of the magnetic measurements and the other thin sections were cut for ordinary petrographic studies.

Chemical analysis, microscopic and field data from Malayer granitoid rocks revealed that they are composed of many various petrologic phases and for simplifying we classify them into three major unites; Syenogranite, Monzogranite and Granodiorite. Hereafter the malayer granitoid rocks are consist of mentioned three unites. Because of mafic and intermediate unites have different geochemical history we relinquish them in this stage. Hand specimen mostly show a very high content of hornblendes and biotites giving the rocks a dark grey appearance. The well developed foliation plane in most of the samples is defined by biotites and/or hornblendes. Feldspars are oriented in the foliation plane and sometimes appear to define augen gneisses, however, this texture is only weakly developed. Biotites of the syenogranites are much smaller than biotites in the other suites, they hardly exceed 0.3 cm in diameter.

Syenogranites: This unit has elongate shape that is located parallel to the granodiorite unit (Fig. 4a). Its texture is granular to porphyroid and because of mafic mineral portion is very low they have more brightness than other units. Microcline (10-30%), orthoclase (10-30%), quartz (30-40%) and plagioclase (10-15%) are the major minerals. The accessory minerals are consist of biotite, garnet, tourmaline, amphibole, epidote, sphene, zircon and apatite. Alteration of primary minerals forms secondary minerals such as muscovite, zoisite, clay minerals, chlorite and Fe-oxides. The microperthitic texture observed in microclines and their weak alignment is frequently used as an indicator for deformation in the magmatic state (e.g., Roig *et al.*, 1998; Paterson *et al.*, 1989).

Monzogranites: The field and microscopic characterizations of this type of granite is similar to syenogranite unit but mafic minerals and schistosity are more than those syenogranite. K-feldspar in the monzogranites occurs as euhedral to subhedral grains that frequently show exsolution lamellas of albite (microcline with microperthitic texture) (Fig. 4b). Sericitization in feldspars is common and sericitized grains reflect the zoning.

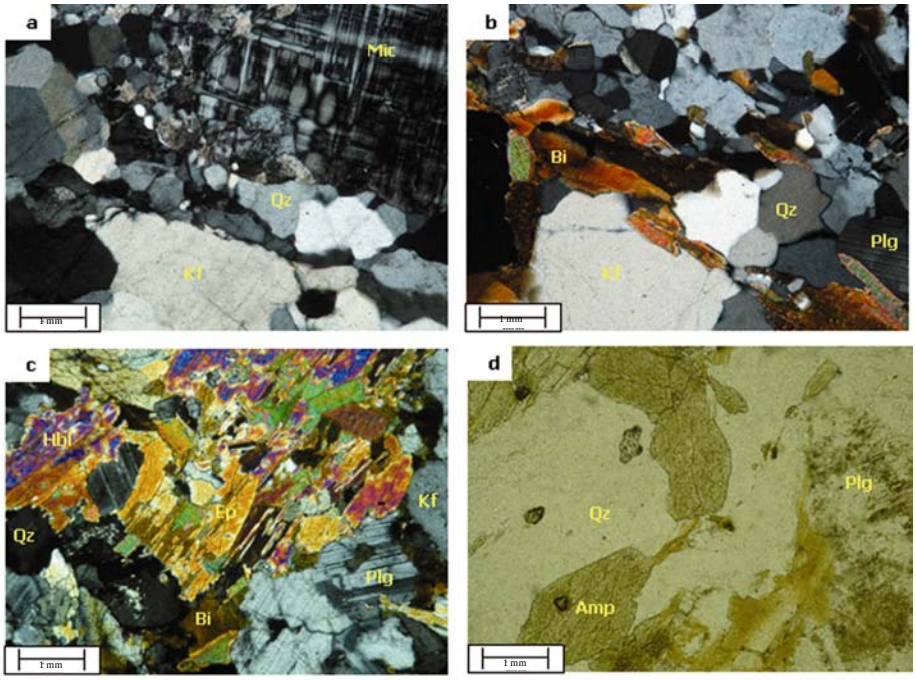

Fig. 4: (a) Syenogranite. XPL (b) Monzogranite. XPL (c) Granodiorite. XPL and (d) Tonalite. PPL, Mic: Microcline, Qz: Quartz, Kf: Potassic Feldspar, Bi: Biotite, Plg: Plagioclase, Hbl: Hornblende, Ep: Epidote, Amp: Amphibole

Myrmekites can frequently be observed around feldspars. The abundant sub- to euhedral biotites in the mozogranites occur in a wide variety of grain sizes and resemble the typical birds-eye structures. Hornblendes occur as cluster of small, euhedral grains that do not show any signs of twinning or as larger, euhedral to subhedral grains.

Granodiorites: The widespread granodiorite unit ranges in composition from tonalite to granodiorite and monzodiorite forms a large ellipsoid NW-extending pluton. These rocks have mainly granular and minority porphyritic texture (Fig. 4c, d). Their mineralogical assemblage is: plagioclase (20-50%), quartz (10-40%), alkali feldspar (mostly microcline) (5-15%), biotite (5-30%) and amphibole (5-15%). Zircon, apatite, sphene, epidote, allanite and opaque minerals are the accessory minerals. In some sample secondary muscovite is present. Zircon and apatite are present as inclusion in the biotite and plagioclase minerals. Amphibole and biotite are the main mafic minerals in these rocks and pyroxene is rare. In some samples, biotite content is over 30% and rocks colour is dark brown due to this minerals. Alteration of amphibole form the secondary biotite. Sphene and zircon are euhedral. Plagioclase has polysynthetic macle and zoned structure. Sosoritization of plagioclases is the common process that forms sericite, clinozoisite and calcite. Plagioclases are undergone mechanical crash and their crash zones are filled by quartz and alkali feldspar. Alkali feldspars are in form of microcline and perthite. Alkali feldspar and quartz show oscillatory distinction. Myrmekitic and mylonitic textures are common. In the hand samples the coarse minerals such as quartz, alkali feldspar and biotite can be seen. Orientation of biotite and amphibole cause to an obvious schistosity in these rocks specially at the corner of the complex.

Petrofabric and field observations: Field observations of the Malayer granites revealed numerous small scale shear zones (Ahadnejad *et al*., 2008). The shear zones often cut xenoliths with offsets of a few centimeters (Fig. 5). Kinematic indicators in these small scale shear zones show dextral movements and therefore probably originated from movement along the Shear Zone. It is obvious from the hand specimen as well as from thin sections and field observations that the amount of deformation seems to decrease towards the body center.

Granitoids: There are so many wartlike myrmekitic textures in the complex that demonstrate affect of stress during granitoid emplacement. Myrmekite is an intergrowth of vermicular quartz and sodic plagioclase

Fig. 5: Xenolith crosscut and offset by a small shear zone which filled by the tourmaline granite

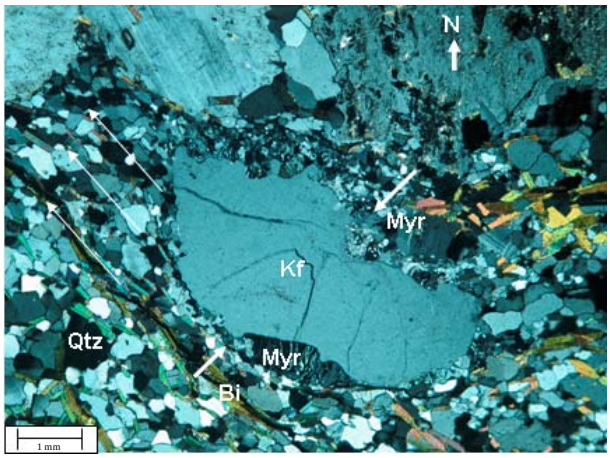

Fig. 6: Myrmekitic texture. Short thick arrows show the shortening side of coarse feldspar and long thin arrows show the foliation. N shows the north. XPL Qtz: Quartz, Kf: Potassic Feldspar, Bi: Biotite, Myr: Myrmekite, N: Geographic North

which occurs near the rim of a plagioclase crystal, either between grains of perthitic K-feldspar or along the contact of K-feldspar and plagioclase crystals (Turner and Verhoogen, 1960; Phillips, 1974; Cox *et al*., 1979). Wartlike myrmekite is produced where the deformation is strong and always occurs with abundant microcline or orthoclase. Simpson and Wintsch (1989) showed that this kind of myrmekite only form in sides that are perpendicular to shortening in the coarse feldspars (Fig. 6). By comparing of shorter diameter and stress direction results from study of fault and sutures confirm this subject. Furthermore, biotite, amphibole andalusite, turmaline and feldspar orientation are fallowed from intrusive body foliation (Fig. 4a, b, 7). The domain of granitic rocks have a foliation parallel to orientation of country metamorphic rocks.

Existing mylonitic granites along the shear zones of body are the important sign of shearing deformation at the granodiorites (Fig. 8a-c). Feldspars that could not undergo the plastic deformation crushed due to shearing type deformation. At the second pulse of injection, light colour syenogranites are injected at the shear zones. For example, injection of tourmaline-granite as thin layers in the main body cause to differential layering with layers full of tourmaline and quartz-feldspar (Fig. 8a). Field observations demonstrate that injection of the locogranites is simultaneous to second step of faulting and shearing. Granitoid that not underwent deformation

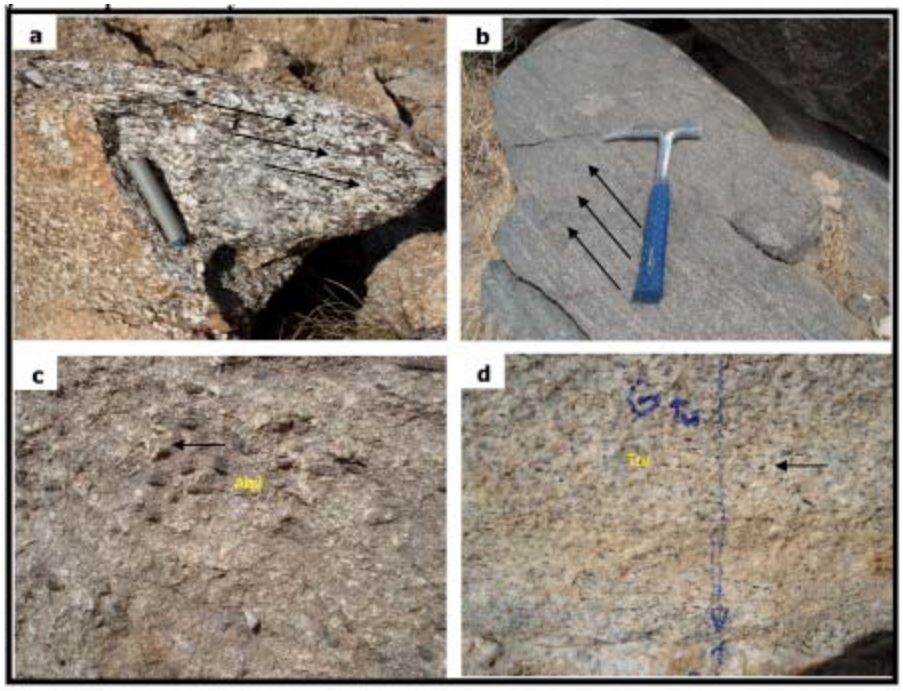

Fig. 7: (a-b) Field observations show strong alignment of biotites. foliation direction (arrows). (c-d) orientation of minerals andalusite and tourmaline, respectively. And: Andalusite, Tur: Turmaline

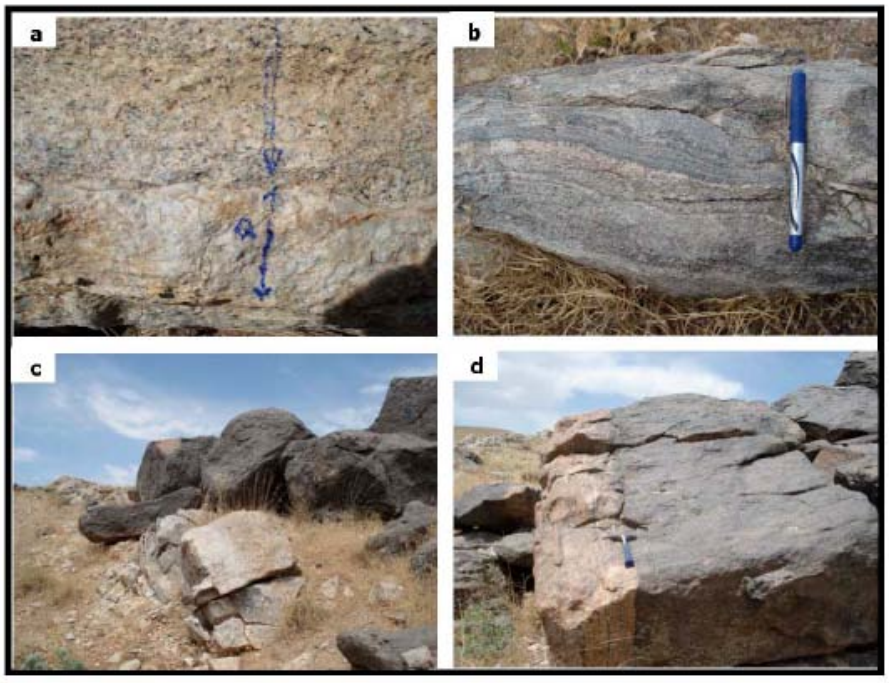

Fig. 8: Local shear zones in the Malayer granitoid complex. (a) Injection of tourmaline-granite into the main granitic body and formation of differential layering, (b) Migmatitic granite, (c) Injection of locogranite in the shear zone and (d) Mylonitization in the shear zone

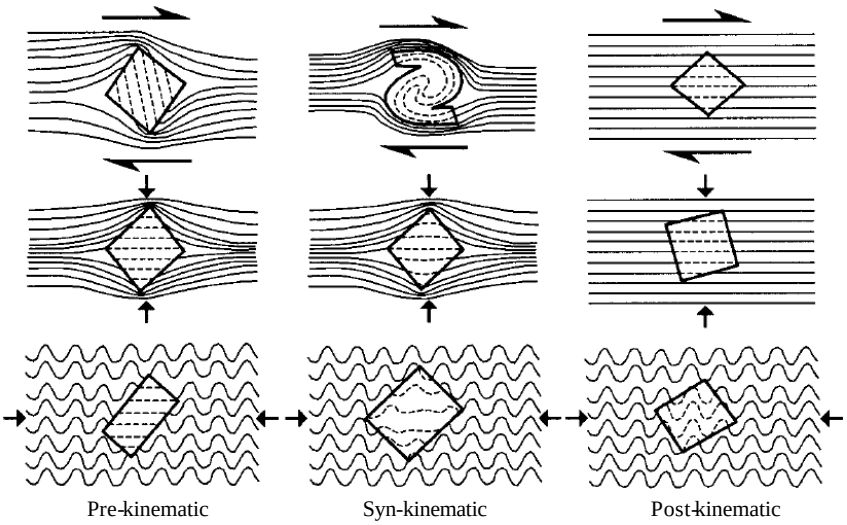

Fig. 9: Diagram of pre-, syn- and post-tectonic porphyroblasts. Pre-tectonic where porphyroblast inclusion trails are generally discordant to those of matrix. Syn-tectonic where inclusion trails indicating deformation during growth. Post-tectonic where porphyroblasts clearly grow after a previously developed matrix foliation and inclusion trails are generally consistent with those of matrix. After Johnson (1999)

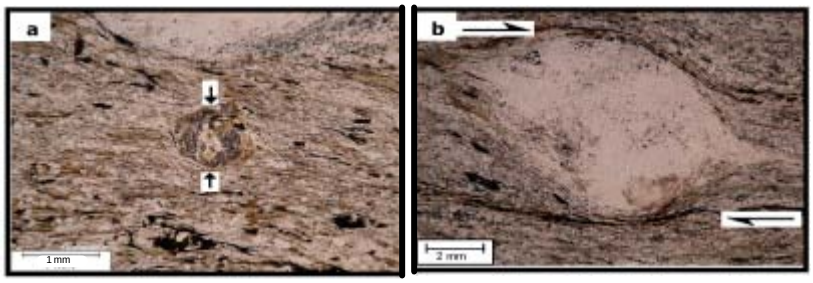

Fig. 10: Porphyroblasts of regional metamorphic rocks indicate syn-tectonic deformation. (a) Garnet and (b) Starulite

could be shown injection of magma at the end of shearing deformation or high liquid quantity in the magm a. If magmatic body is emplaced by bulk magmatic flow, then during emplacement, the magma must contain a melt fraction of at least 30-40 vol.% (Vignersse *et al.*, 1996). At lower melt fractions, crystals in the melt are welded to their neighbors. Composition of magma flow and regional deformation cause to foliation in the igneous body (Paterson *et al.*, 1991). In the interested area, because of going beyond of crystallization in the body corners, shearing of crystals and crystal mush and transferring of k-feldspar rich fluids into the low stress parts of shear zone cause to sequential locogranite and tonalitic layers that be a characteristic as existing and absence of microcline, respectively.

Metamorphic rocks: In order to understand the relationships between metamorphic mineral growth and deformation in the Malayer igneous complex, studies of microstructural textures were conducted, focusing on porphyroblast-matrix relationships. Small-scale microstructural features in metamorphic rocks provide important information on the relative timing of deformation and metamorphic mineral growth. This information is very useful in interpreting the tectonic setting of metamorphism. Perhaps the most useful tool for interpreting relationships between deformation and metamorphism are porphyroblasts and their relationships to deformational fabrics within a rock. Porphyroblasts are mineral grains (e.g., garnet, staurolite, etc.) that are significantly larger than those of the surrounding matrix and because they are typically harder and more resistant to deformation, they often preserve earlier structures (Fig. 9).

Microstructureal studies of regional metamorphic rocks in the Malayer indicate that the injection of granitic magma into the country rocks is syn to post-tectonic. Syn-tectonic indicating porphyroblast growth synchronous with the development of the external fabric (Fig. 10). The thermal contact area of the granite can be

observed in the contact margin of granite and regional metamorphic rocks, where it produced hornfelses and local feldspatisation.

ENCLAVES

Microgranitoid and xenolithic enclaves are very common in the interested granitoids. Microgranitoid enclaves composition is felsic to intermediate (mostly tonalitic in composition) and shape is various from elongated and ellipsoid in margin area and egded to circular in the rest of body. (Fig. 11). They are finer-grained and typically have more mafic portions than the host granite. These enclaves range from centimetres up to decimetres in size. Xenolithic enclaves are same as country rocks in chemical composition and schistosity. The xenolithic enclaves are observed at the contact of granitoids with the metamorphic basement. Their texture and mineral composition reveal that these enclaves are phyllite, schist and hornfels. Reaction narrow haloes can bee seen in these enclaves that indicate their reaction with hot magma.

RESULTS AND DISCUSSION

Lineations are commonly used to determine the direction of tectonic transport in rocks and the strength of such lineations is often taken as an indicator of strain intensity. The Malayer granitoids have a foliation containing a subhorizontal West-Northwest trending stretching lineation and mostly dextral shear-sense criteria. The sigmoidal shape of the rocks confirm this idea (Paterson *et al*., 2004). Horizontal to subhorizontal orientation of structures and features (such as lineations) rule out the diapirisam model. Some major fault zones can be recognized very well, they usually are pathways for rivers draining the area. Their strike is very consistent, either NE-SW or W-E. Mylonitic shear zones usually were found locally at the pluton´s rim.

The macroscopic foliation in the granitoid rocks of the Malayer granitoids are parallel to the country metamorphic rocks (NW-SE). This indicates nearly coeval emplacement of the granitoids and a major deformation phase of the different metamorphic rocks. The microscopic analyzes showed that a division of the

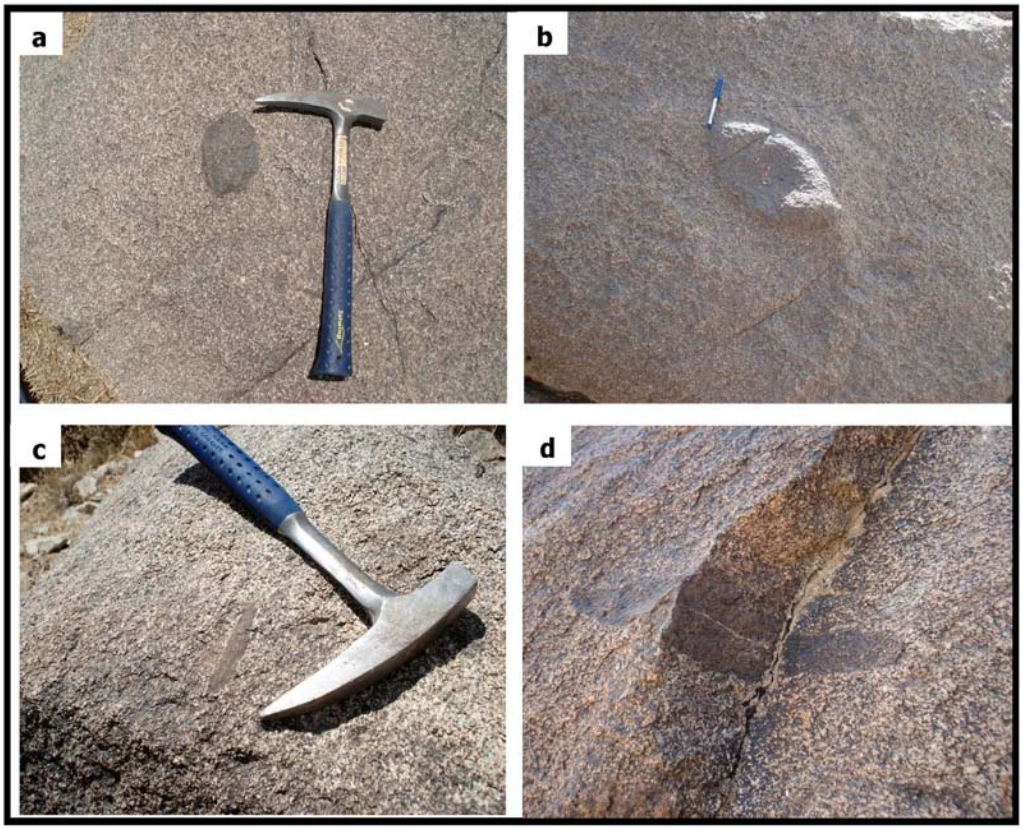

Fig. 11: Microgranitoid (a and b) and Xenolithic Enclaves in the different localities of the complex (a) circular, (b) ellipsoid, (c) elongated and (d) enclave is oriented in the foliation plane

different location of the Malayer complex according to their amount of deformation can be drawn. Marginal areas of the granitoids show the highest deformational while the central parts only show a weak overprint of magmatic features. The microstructures observed in felsic granites are comparable to those of the mafic granites. The mafic granites show generally a distinct foliation due to orientation of mafic minerals such as biotite and amphibole and felsic granites show this foliation by orientation of feldspar and quartz.

Microscopic studies and field observations demonstrate that magma ascent and emplacement are rapid. For example, For epidote crystals to have been preserved as found in the granites of the Malayer required a rapid ascent rate. Such a rapid ascent rate is similar to magma transport rates in shear zones. Because of the rapid ascent rates, chemical and thermal interaction between magmas and the surrounding country rocks will be minimal. Oscillatory zoning is weakly developed and widely spaced documenting the rapid growth during crystallization. Transpression regime which demonstrated by most of these structures and features is the best tectonic model for the emplacement of the Malayer complex.

ACKNOWLEDGMENT

This research was supported by Iran National Science Foundation Grant No. 86103/32.

REFERENCES

Ahadnejad, V., M.V. Valizadeh and D. Esmaeily, 2008. Shear zone control on the emplacement of Malayer granitoid complex. NW Iran, Joint Meeting of the GSA. http://gsa.confex.com/gsa/2008AM/final program/abstract_144093.htm.

Ahmadi Khalaji, A., D. Esmaeily, M.V. Valizadeh and H. Rahimpour-Bonab, 2006. Petrology and geochemistry of the granitoid complex of Boroujerd, Sanandaj-Sirjan Zone, Western Iran. J. Asian Earth Sci., 29: 859-877.

Alavi, M., 1994. Tectonics of the Zagros Orogenic belt of Iran: New data and interpretations. Tectonophysics, 229: 211-238.

Barker, F. and J.G. Arth, 1976. Generation of trondhjemitic-tonalitic liquids and Archean bimodal trondhjemite-basalt suites. Geology, 4: 596-600.

Berberian, F. and M. Berberian, 1981. Tectono-Plutonic Episodes in Iran. In: Zagros. Hindu Kush, Himalaya Geodynamic Evolution, Gupta, H.K. and F.M. Delany (Eds.). American Geophysical Union, Geodyn. Ser., 3, Washington, DC, ISBN:0875905072, pp: 5-32.

Brown, M. and G.S .Solar, 1998. Shear zones and melts: Positive feedback in orogenic belts. J. Struct. Geol., 20: 211-227.

Clemens, J.D. and C.K. Mawer, 1992. Granitic magma transport by fracture propagation. Tectonophysics, 204: 339-360.

Clemens, J.D., N. Petford and C.K. Mawer, 1997. Ascent Mechanisms of Granitic Magmas: Causes and Consequences. In: Deformation-Enhanced Fluid Transport in the Earth's Crust and Mantle, Holness, M. (Ed.). Chapman and Hall, London, ISBN: 0-412-75290-5 pp: 145–172.

Collins, W.J. and E.W. Sawyer, 1996. Pervasive granitoid magma transport through the lower-middle crust during non-coaxial compressional deformation. J. Metamorphic Geol., 14: 565-579.

Cox, K.G., J.D. Bell and R.J. Pankhurst, 1979. The Interpretation of Igneous Rocks. 1st Edn. George Allen and Unwin Ltd., London, ISBN: 0045520151, pp: 445.

D'Lemos, R.S., M. Brown and R.A. Strachan, 1993. Granite magma generation, ascent and emplacement within a transpressional orogen. J. Geol. Soc. London, 149: 487-490.

Hatzfeld, D., M. Tatar, K. Priestley and M. Ghafory-Ashtiany, 2003. Seismological constraints on the crustal structure beneath the Zagros Mountain belt (Iran). Geophys. J. Int., 155: 403-410.

Holdsworth, R.E., C.A. Butler and A.M. Roberts, 1997. The recognition of reactivation during continental deformation. J. Geol. Soc. London, 154: 73-78.

Hutton, D.H.W., 1997. Syntectonic Granites and the Principle of Effective Stress: Ageneral Solution to the Space Problem? In: Granite: From Segregation of Melt to Emplacement Fabrics, Bouchez, J.L., D.H.W. Hutton and W.E. Stephens (Eds.). Kluwer Academic Publishers, Dordrecht, Netherlands, ISBN: 0-7923-4460-X, pp: 189-197.

Irvine, T.N. and W.R.A. Baragar, 1971. A guide to the chemical classification of the common volcanic rocks. Can. J. Earth Sci., 8: 523-548.

Johnson, S.E., 1999. Porphyroblast microstructures: A review of current and future trends. Am. Mineral, 84: 1711-1726.

Mazhari, S.A., F. Bea, S. Amini and J. Ghalamghash, 2008. Estimation of pressure and temperature of intrusive rocks crystallization: A case study of Naqadeh, Pasveh and Delkeh plutons, W Iran. J. Applied Sci., 8: 934-945.

Mohajjel, M., C.L. Fergusson and M.R. Sahandi, 2003. Cretaceous-Tertiary convergence and continental collision, Sanandaj-Sirjan Zone, Western Iran. J. Asian Earth Sci., 21: 397-412.

Paterson, S.R., R.H. Vernon and O.T. Tobisch, 1989. A review of criteria for the identification of magmatic and tectonic foliation in granitoids. J. Struct. Geol., 11: 349-363.

Paterson, S.R., R.H. Vernon and O.T. Tobisch, 1991. Emplacement and deformation of granitoids during volcanic arc construction in the Foothills terrane, central Sierra Nevada, California. Tectonophysics, 191: 89-110.

Paterson, S.R. and K.L. Schmidt, 1999. Is there a close spatial relationship between faults and plutons? J. Struct. Geol., 21: 1131-1142.

Paterson, S.R., G.S. Pignottaa and R.H. Vernon, 2004. The significance of microgranitoid enclave shapes and orientations. J. Struct. Geol., 26: 1465-1481.

Pearce, J.A., N.B.W. Harris and A.G. Tindle, 1984. Trace element discrimination diagrams for the tectonic interpretation of granitic rocks. J. Petrol., 25: 956-983.

Peccerillo, A., and S.R. Taylor, 1976. Geochemistry of eocene calc-alkaline volcanic rocks from the Kastamonu area, Northern Turkey. Contribut. Mineral. Petrol., 58: 63-81.

Petford, N., J.R. Lister and R.C. Kerr, 1993. The ascent of felsic magmas in dykes. Lithos, 32: 161-168.

Petford, N., A.R. Cruden, K.J.W. McCaffrey and J.L. Vigneresse, 2000. Granite magma formation, transport and emplacement in the earth's crust. Nature, 408: 669-673.

Phillips, E.R., 1974. Myrmekite-one hundred years later. Lithos, 7: 181-194.

Roig, J.Y., M. Faure and C. Truffert, 1998. Folding and granite emplacement inferred from structural, strain, TEM and gravimetric analyzes: The case study of the Tulle antiform, SW French Massif Central. J. Struct. Geol., 20: 1169-1189.

Sarkarinejad, K. and A. Azizi, 2007. Slip Partitioning and inclined dextral transpression along the Zagros Thrust System, Iran. J. Struct. Geol., 30: 116-136.

Sibson, R.H., 1977. Fault rocks and fault mechanisms. J. Geol. Soc. London, 133: 191-213.

Simpson, C. and R.P. Wintsch, 1989. Evidence for deformation-induced K-feldspar replacement by myrmekite. J. Metamorphic Geol., 7: 261-276.

Snelling, A.A., 2008. Catastrophic granite formation: Rapid melting of source rocks and rapid magma intrusion and cooling. Answer Res. J., 1: 11-25.

Turner, F.J. and J. Verhoogen, 1960. Igneous and Metamorphic Petrology. 2nd Edn. McGraw-Hill Publishing Company, New York, ISBN: 070655790, pp: 694.

Vigneresse, J.L., P. Barbey and M. Cuney, 1996. Rheological transitions during partial melting and crystallization with application to felsic magma segregation and transfer. J. Petrol., 37: 1579-1600.

Vigneresse, J.L. and B. Tikoff, 1999. Strain partitioning during partial melting and crystallizing felsic magmas. Tectonophysics, 312: 117-132.

Vigneresse, J.L. and J.D. Clemens, 2000. Granitic Magma Ascent and Emplacement: Neither Diapirism nor Neutral Buoyancy. In: Salt, Shale and Igneous Diapirs in and Around Europe, 174, Vendeville, B., Y. Mart and J.L. Vigneresse (Eds.). Geol. Soc. London Spec. Publ., London, pp: 1-19.

Weinberg, R.F. and Y. Podladchikov, 1994. Diapiric ascent of magmas through power law crust and mantle. J. Geophys. Res., 99: 9543-9559.

White, S.H., S.E. Burrows, J. Carreras, N.D. Shaw and F.J. Humphreys, 1980. On mylonites in ductile shear zones. J. Struct. Geol., 2: 175-187.

Wilson, M., 1989. Igneous Petrogenesis. 1st Edn. Unwin Hyman, London, ISBN: 0045520240 0045520259.